



AFRL-OSR-VA-TR-2013-0138

**Plasmonic Structures for CMOS Photonics and Control of
Spontaneous Emission**

**Harry A. Atwater
California Institute of Technology**

**April 2013
Final Report**

DISTRIBUTION A: Approved for public release.

**AIR FORCE RESEARCH LABORATORY
AF OFFICE OF SCIENTIFIC RESEARCH (AFOSR)
ARLINGTON, VIRGINIA 22203
AIR FORCE MATERIEL COMMAND**

REPORT DOCUMENTATION PAGE

Form Approved
OMB No. 0704-0188

Public reporting burden for this collection of information is estimated to average 1 hour per response, including the time for reviewing instructions, searching existing data sources, gathering and maintaining the data needed, and completing and reviewing this collection of information. Send comments regarding this burden estimate or any other aspect of this collection of information, including suggestions for reducing this burden to Department of Defense, Washington Headquarters Services, Directorate for Information Operations and Reports (0704-0188), 1215 Jefferson Davis Highway, Suite 1204, Arlington, VA 22202-4302. Respondents should be aware that notwithstanding any other provision of law, no person shall be subject to any penalty for failing to comply with a collection of information if it does not display a currently valid OMB control number. **PLEASE DO NOT RETURN YOUR FORM TO THE ABOVE ADDRESS.**

1. REPORT DATE (DD-MM-YYYY) 2/1/2013		2. REPORT TYPE Final Performance Report		3. DATES COVERED (From - To) July 1, 2009 – July 1, 2012	
4. TITLE AND SUBTITLE Plasmonic Structures for CMOS Photonics and Control of Spontaneous Emission				5a. CONTRACT NUMBER	
				5b. GRANT NUMBER FA9550-09-1-0673	
				5c. PROGRAM ELEMENT NUMBER	
6. AUTHOR(S) Harry A. Atwater				5d. PROJECT NUMBER	
				5e. TASK NUMBER	
				5f. WORK UNIT NUMBER	
7. PERFORMING ORGANIZATION NAME(S) AND ADDRESS(ES) California Institute of Technology 1200 E. California Blvd. Pasadena, CA 91125				8. PERFORMING ORGANIZATION REPORT NUMBER	
9. SPONSORING / MONITORING AGENCY NAME(S) AND ADDRESS(ES) Air Force Office of Scientific Research 875 N. Randolph St. Arlington, VA 22203 Dr. Gernot S. Pomrenke				10. SPONSOR/MONITOR'S ACRONYM(S)	
				11. SPONSOR/MONITOR'S REPORT NUMBER(S) AFRL-OSR-VA-TR-2013-0138	
12. DISTRIBUTION / AVAILABILITY STATEMENT Distribution A: Approved for public release					
13. SUPPLEMENTARY NOTES					
14. ABSTRACT In this project, we have i) demonstrated modulation of the refractive index $\Delta n > 1$ at near infrared frequencies during field effect gating of conducting oxide (ITO) thin films for switching applications; ii) demonstrated record low coupling loss from silicon-on-insulator waveguides to dielectrically-loaded surface plasmon polariton waveguides with 1 dB/transition insertion loss and also metal-insulator-metal waveguides; iii) developed a full format CMOS image sensor with plasmonic color filters; iv) explored enhanced spontaneous emission in nanoscale plasmonic cavities and have experimentally observed enhanced spontaneous emission in polymer plasmonic structures; v) developed CMOS Si photonic switching device based on the vanadium dioxide (VO ₂) phase transition. vi) also engaged in a partnership with the CEA-LETI laboratory and developed a next generation plasMOSstor plasmonic metal-insulator-metal device in CMOS Si photonics with copper metallization and SOI waveguide-coupled inputs and outputs.					
15. SUBJECT TERMS					
16. SECURITY CLASSIFICATION OF:			17. LIMITATION OF ABSTRACT	18. NUMBER OF PAGES	19a. NAME OF RESPONSIBLE PERSON G. Pomrenke
a. REPORT U	b. ABSTRACT U	c. THIS PAGE U			19b. TELEPHONE NUMBER (include area code) 703-696-8426

Project Summary:

In the last ten years, significant advances have been made in both the Si CMOS photonic and optoelectronics fields, as well as a rapid growth in understanding of plasmonics. The aim of this project was to explore the nanophotonic interface between chip-based CMOS Si photonic structures and plasmonics. At the outset of the project in 2009, a ‘first wave’ of development of plasmonic nanoscale structures was reaching full development. At the start of the grant period, important outstanding challenges at the photonics/plasmonic interface included the ability

- to efficiently couple light at telecommunication wavelengths from free space or from Si photonic networks into plasmonic waveguides, as well as
- to develop an understanding of active optical switching mechanisms in nanoscale plasmonic structures and to
- to mitigate losses in plasmonic structures through introduction of new materials and via photonic design.

Over its three year span, the project demonstrated several key advances in understanding of plasmonic structures for enhancement of spontaneous emission and for efficient coupling of light into Si-based nanostructure structures for CMOS photonic and optoelectronic applications, as well as other advances. Key project outcomes include:

- i. demonstrating of modulation of the refractive index $\Delta n > 1$ at near infrared frequencies during field effect gating of conducting oxide (ITO) thin films, of considerable interest for switching applications;
- ii. demonstration of record low coupling loss from silicon-on-insulator waveguides to dielectrically-loaded surface plasmon polariton waveguides with < 1 dB/transition insertion loss,
- iii. efficient coupling from silicon-on-insulator waveguides to metal-insulator-metal plasmon waveguides with 1 dB/transition insertion loss.
- iv. development of a full-format CMOS image sensor with plasmonic color filters and demonstration of imaging.
- v. Design of a plasMOSstor plasmonic switching device, with low insertion loss, implemented in CMOS Si photonics with copper metallization and SOI waveguide-coupled inputs and outputs, in a partnership with the CEA-LETI laboratory.
- vi. Developing a CMOS Si photonic switching device based on the vanadium dioxide (VO_2) phase transition.
- vii. exploring approaches to enhance spontaneous emission in nanoscale plasmonic cavities and experimentally observing enhanced spontaneous emission in GaAs and polymer plasmonic antenna structures.

These developments have clear potential for further development of ultralow power and CMOS detector arrays. The findings related to field effect switching of refractive index in conducting oxides is the basis of current efforts to develop high-speed nanoscale plasmonic switches and circuits. The advances in efficient insertion and coupling between plasmonic and Si photonic waveguides has stimulated a new effort by Atwater under AFOSR Hybrid MURI support to investigate ultra compact plasmonic/photonic hybrid devices and circuits. The work on plasmonic color filters for CMOS imaging arrays has spawned a collaboration with Sony to investigate large-scale hyperspectral and polarimetric imaging arrays based on integration of plasmonic filters with state-of-the-art CMOS image sensors.

By way of enumeration, 13 journal papers were published under AFOSR grant support, and these have already been cited collectively more than 250 times (Google Scholar). The principal investigator Harry Atwater gave 82 invited talks in international conferences, workshops, and university colloquia, including the MRS Kavli Lecture (2010), the Plasmonics Gordon Conference (2009 & 2011), the Ehrenfest Colloquium at the Lorenz Institute in Leiden, and at the 2010 TED conference, as well as Group IV Photonics and the Physics of Quantum Electronics. Atwater was awarded the Fred Kavli Distinguished Nanoscience Award in 2010 by the MRS, and the Eni Award and SPIE Green Photonics Award at Photonics West in 2012.

During the project, five graduate students and one postdoc received significant support. Dr. Carrie Hofmann and Dr. Ryan Briggs earned PhD degrees from Caltech in Materials Science. Dr. Imogen Pryce earned a PhD in Chemical Engineering. Current students Stanley Burgos and James Fakonas were also supported under the grant. Briggs is currently a member of technical staff at the Jet Propulsion Laboratory, working on mid-infrared photodetectors. Hofmann is currently Assistant Director of the Light-Material Interactions Energy Frontier Research Center. Pryce currently is a technology analyst for Boston Consulting Group. Dr. Koray Aydin was supported as a postdoctoral scholar; Aydin is currently an Assistant Professor of Electrical Engineering at Northwestern University. Burgos will join Hitachi Global Storage as a technical staff member in 2013 working on plasmonic structures for high-density heat-assisted magnetic recording applications.

Accomplishments under Project:

Researchers have recently demonstrated important optical components on SOI, including lasers and photodetectors operating at wavelengths near 1550 nm. Thus, while plasmonic waveguide circuitry has great potential for architectures with unique functionality, integration on SOI can facilitate the realization of on-chip plasmonic devices that take advantage of components already developed for Si photonics. Furthermore, SOI waveguides can serve as low-loss interconnects for moving light between miniaturized plasmonic devices, minimizing overall on-chip losses.

Compared with dielectric waveguides, propagating surface-plasmon waveguides can confine light to smaller volumes and enhance light-matter interaction, but they suffer from metal-induced propagation loss. The impact of signal propagation loss on cm^2 -scale integrated photonic chips can be minimized using an architecture featuring short plasmonic waveguides coupled to longer dielectric waveguides. This design approach significantly reduces overall chip-level waveguide losses relative to all-plasmonic networks, but the development of low-loss transitions between plasmonic and dielectric waveguides becomes critical.

Efficient Coupler between Si Photonic and Metal-Insulator-Metal Plasmonic Waveguides

Metal-insulator-silicon-metal (MISM) hybrid plasmonic waveguides are of particular interest for active CMOS plasmonics because they support highly confined modes and can potentially be integrated with standard processes used in silicon-based electronics foundries. However, such plasmonic structures must balance high field confinement with optical losses. Minimizing metal-related optical losses for integrated plasmon-assisted devices remains a key issue that can be addressed through both material selection and careful design of waveguide geometries. Considering the latter, the mode size mismatch and difference in phase index between standard silicon-on-insulator (SOI) photonic waveguides and metal-insulator-metal waveguides lead to high coupling losses. To overcome this issue, several coupling configurations have been proposed previously, including optimized butt couplers, taper couplers, and directional couplers.

We have experimentally realized a compact, efficient coupler between silicon waveguides and vertical metal-insulator-silicon-metal (MISM) plasmonic waveguides, shown in Fig. 1. Devices were fabricated using complementary metal-oxide-silicon (CMOS) technology processes, with copper layers that support low-loss

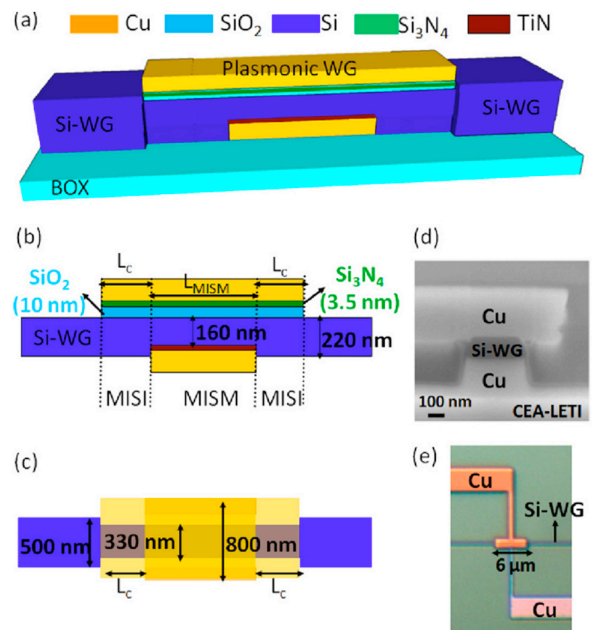


Figure 1. (a) Three-dimensional view of the investigated hybrid plasmonic waveguide. (b) Side and (c) top views showing the coupling structure (MISI) connecting the SOI and plasmonic (MISM) waveguide sections. (d) SEM image of the cross section of the MISM plasmonic waveguide. (e) Optical microscope image (top view) of the fabricated plasmonic structure integrated with silicon waveguides.

plasmonic modes in the MISM structures at a wavelength of 1550 nm. By implementing a short (0.5 μm) optimized metal-insulator-silicon-insulator structure inserted between the photonic and plasmonic waveguide sections, we demonstrate experimental coupling loss of 2.5 dB, despite the high optical confinement of the MISM mode and mismatch with the silicon waveguide mode. The observed attenuation is a factor of three smaller than the value measured for directly coupled photonic and plasmonic waveguides, and is attributed to multimode interference effects between the waveguide mode and the plasmonic edge mode within the short coupling structure.

Efficiently Coupling between Plasmonic and Silicon Photonic Waveguides

In this work, we demonstrate dielectric-loaded surface plasmon polariton (DLSPP) waveguides coupled to SOI waveguides with transition losses as low as 1 dB. Grating-coupled SOI ridge waveguides were aligned to polymer-on-Au DLSPP sections using multiple aligned electron-beam lithography steps, as depicted schematically in Fig 2(a). The Au regions are recessed below the top surface of the SOI waveguides, as shown in the scanning electron micrograph in Fig. 2(c), allowing for ideal coupling between the transverse-magnetic (TM) mode of the SOI waveguide and the surface plasmon mode supported on the Au surface. PMMA electron-beam resist was patterned as a cover layer for the SOI waveguides and as a dielectric load for laterally confining surface plasmons on the Au surface, as shown in Fig. 2(b). The PMMA was patterned to form straight DLSPP waveguide sections and evanescently coupled DLSPP ring resonators, shown in Fig. 2(d)-(e).

In addition to supporting a fundamental TM mode that couples strongly to TM-polarized surface plasmons, the SOI waveguides fabricated here support a transverse-electric (TE) mode. The modes can be accessed selectively by adjusting the input/output grating coupling angle, θ , defined in Fig. 2(a). Figure 3(b) shows transmission spectra for SOI-DLSPP waveguide devices with DLSPP sections of varying length. The top panel shows the transmission through a SOI waveguide reference device with no DLSPP section and a series of devices with a DLSPP section ranging in length between $L = 10$ and $50 \mu\text{m}$, where light near $\lambda = 1550 \text{ nm}$ was coupled into the TM SOI waveguide mode at a coupling angle of $\theta = -26.5^\circ$. The lower panel shows that when light is coupled into the TE-polarized SOI waveguide mode at a coupling angle of $\theta = 26^\circ$, there is strong transmission through the reference device, but substantially reduced transmission through even the shortest SOI-DLSPP device. This demonstrates that, as expected, only the TM-polarized SOI waveguide mode couples efficiently to surface plasmons and, furthermore, that there is very little transmission due to coupling to radiation modes. In particular, if light were traversing the Au section between the SOI input/output waveguides via radiation modes, the transmission would not exhibit the strong polarization dependence observed here.

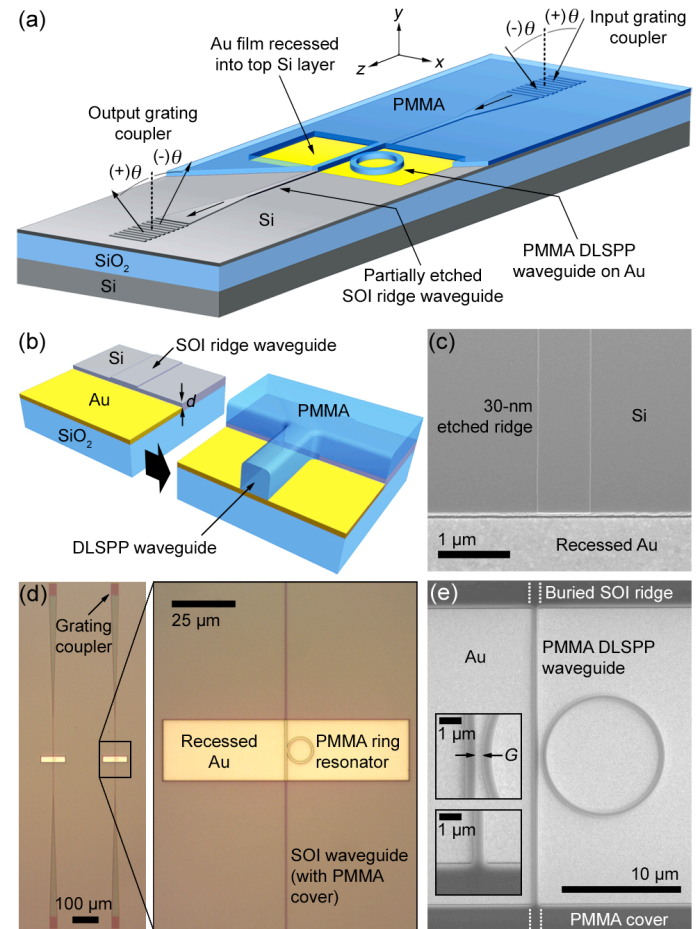


Figure 2. (a) Schematic of a SOI-waveguide-coupled DLSPP waveguide and ring resonator. For clarity, the PMMA layer is shown partially removed from the output SOI waveguide. (b) Scale representation of the coupling region between end-coupled SOI and DLSPP waveguides before and after spinning and patterning of the PMMA cover layer. (c) Scanning electron micrograph of an etched Si ridge waveguide at the boundary of a recessed Au pad before coating with PMMA. (d) Optical micrographs of completed SOI-waveguide-coupled DLSPP devices. (e) Scanning electron micrograph of a DLSPP waveguide and ring resonator (coupling gap $G = 300 \text{ nm}$) extending between buried SOI waveguides.

In Fig. 3(a), we show the transmission through a series of SOI-DLSPP devices, normalized to the average transmission measured for a set of SOI reference devices. The transmission as a function of DLSPP waveguide length is well reproduced at multiple grating coupling angles and wavelengths, and reveals a surface plasmon propagation length of approximately $L_{SPP} = 50 \mu\text{m}$, which agrees well with calculated values. Furthermore, by extrapolating the trend to a device length of 0, the total in- and out-coupling loss is 2 dB, which suggests a coupling loss of 1 dB per SOI-DLSPP transition. Finally, transmission spectra for DLSPP ring resonator devices (not shown here), demonstrate efficient coupling to plasmonic whispering-gallery modes. The round-trip loss in the ring resonators is increased by substantial bending loss; however, we observe loaded resonator Q factors as high as 140.

We have demonstrated *record low insertion loss for coupling from Si photonic to plasmonic waveguides* using low-loss SOI waveguides and DLSPP plasmon waveguides at telecommunication wavelengths. Propagation loss was determined experimentally using variable-length DLSPP waveguides, and we observed a propagation length of approximately $50 \mu\text{m}$. Compared with the transmission measured through SOI reference waveguides, we determine a per-coupler loss of just 1 dB, which is, to our knowledge, the highest reported coupling efficiency into a dielectric-loaded surface plasmon waveguide. The devices demonstrated here show that DLSPP waveguides can be efficiently interfaced with optical systems fabricated on SOI to combine the confinement of plasmonics with the low propagation loss of Si photonic circuits. Furthermore, with the addition of SOI-integrated light sources and detectors, these plasmonic devices can be integrated into a compact, self-contained optical system on a chip.

Silicon-Photonic Waveguide Modulator Based on the Vanadium Dioxide Phase Transition

In the interest of scalability and cost, there has been a push in recent years to develop Si-based waveguide modulators that are competitive with III-V and LiNbO_3 -based devices. Si-based modulators typically take advantage of small changes in the refractive index of Si due to voltage-induced variations in charge density, which, when integrated with a high-quality cavity Mach-Zehnder interferometer (MZI), can lead to modulation in excess of 15 dB at frequencies on the order of 1 to 10 GHz. However, in order to accommodate interferometric structures, these devices have linear dimensions greater than $10 \mu\text{m}$ and are limited to a narrow spectral range. To overcome these limitations in size and bandwidth, we are exploring phase-change materials and, in particular, vanadium dioxide. VO_2 undergoes an insulator-to-metal phase transition that is accompanied by drastic changes in its optical properties, which facilitates the design of compact and broadband single-pass modulator devices.

The VO_2 phase transition can be induced thermally by heating the material over $68 \text{ }^\circ\text{C}$; however, recent work has demonstrated that the phase transition can also be caused by electrical or optical stimuli. Furthermore,

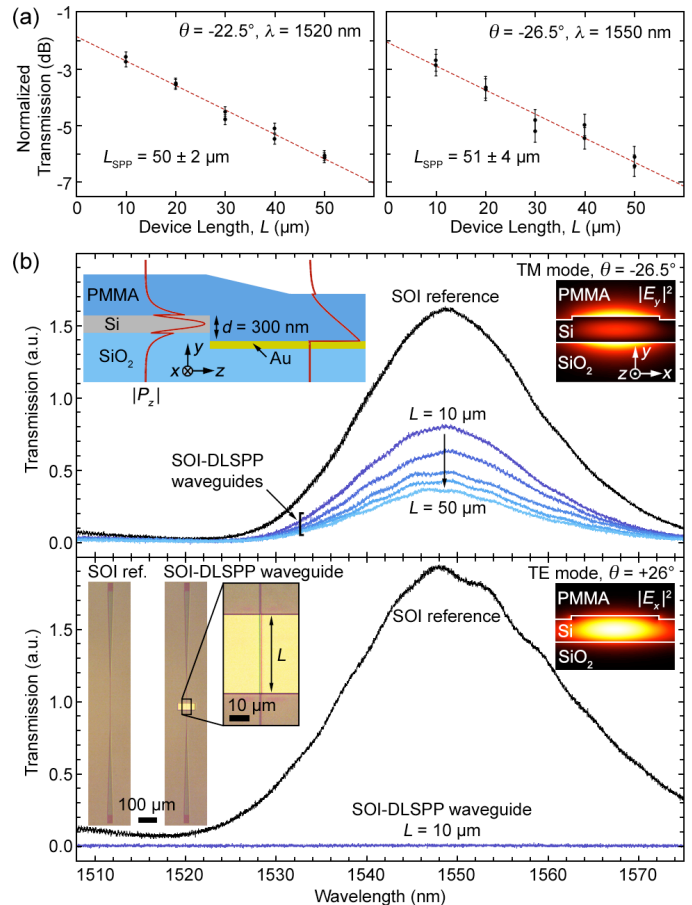


Figure 3. (a) Transmission through a series of SOI-DLSPP waveguide devices as a function of the length, L , of the DLSPP section. The transmission is normalized to the average transmission through a set of three SOI reference devices. The data was collected for the same ten devices at two separate SOI grating coupling angles, θ , and wavelengths, λ , showing that the measured value of the plasmon propagation length, L_{SPP} , is reproducible. (b) Transmission spectra for an SOI reference device and devices with DLSPP sections of varying length. When light is coupled into the TM-polarized SOI waveguide mode, there is significant transmission through the SOI-DLSPP devices; however, when light is coupled into the TE mode of the SOI waveguide, the DLSPP waveguide transmission is greatly reduced.

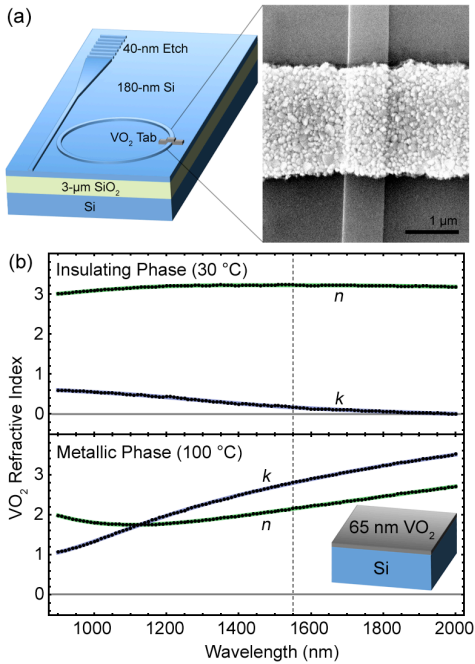


Figure 4. (a) Schematic of the VO₂ modulator test bed, with a grating-coupled through-port waveguide and an evanescently coupled ring resonator. The scanning electron micrograph shows a lithographically defined 2- μm polycrystalline VO₂ tab. (b) Real, n , and imaginary, k , parts of the index of refraction of a VO₂ film on Si measured by spectroscopic ellipsometry for both the insulating and metallic phases.

waveguide devices, we coupled light at wavelengths around 1550 nm into the waveguides using etched surface-relief grating couplers, as depicted in Fig. 4(a). In order to isolate VO₂-induced loss from changes in transmission due to the thermo-optic effect in the Si waveguiding layer, we examined SOI ring resonators, a small portion of which were covered with a VO₂ tab. These resonators support whispering-gallery modes with a spectral line width related to the round-trip cavity loss. As shown in Fig. 5(a) for a reference device with no VO₂ tab, the spectral position of the whispering-gallery mode resonances changes with temperature due to the temperature-dependent index of Si; however, the line width remains constant between 30 and 100 °C. For a device with a 2- μm long VO₂ tab, the line width

the transition can be quite fast when induced athermally, with switching times less than 1 ps observed for the optically triggered insulator-to-metal transformation. However, a significant hurdle to the development useful VO₂-based photonic devices is integration with the conventional Si-on-insulator (SOI) photonics platform. To address this, we have demonstrated a waveguide-integrated VO₂-based modulator fabricated on SOI, with modulation of 6.6 dB over a 2- μm device length. Our device is thermally switched, but it demonstrates the viability of integrating VO₂ on SOI and motivates the development of future devices that take advantage of electrical and optical switching schemes.

To fabricate our waveguide-integrated VO₂ modulator, we patterned low-loss ridge waveguides and ring resonators on SOI using electron-beam lithography and reactive-ion etching. The devices were then covered with a thin film of VO₂ using pulsed-laser ablation of a vanadium metal target in an oxygen ambient. Finally, the VO₂ film was patterned in a second lithography step and etched to define small tabs atop the SOI waveguides, as shown in Fig. 4(a). During the deposition process, VO₂ was also deposited onto a bulk Si substrate for optical characterization by spectroscopic ellipsometry. The complex index of refraction, plotted in Fig. 4(b), was extracted from the 65-nm thick VO₂ film for both the insulating and metallic phases. The material absorption, given by the imaginary part of the index, is relatively low in the insulating phase at a temperature of 30 °C; however, upon heating to 100 °C, the metallic-phase VO₂ film exhibits a 16-fold increase in absorption.

To measure the loss induced by the VO₂ patterned on the SOI

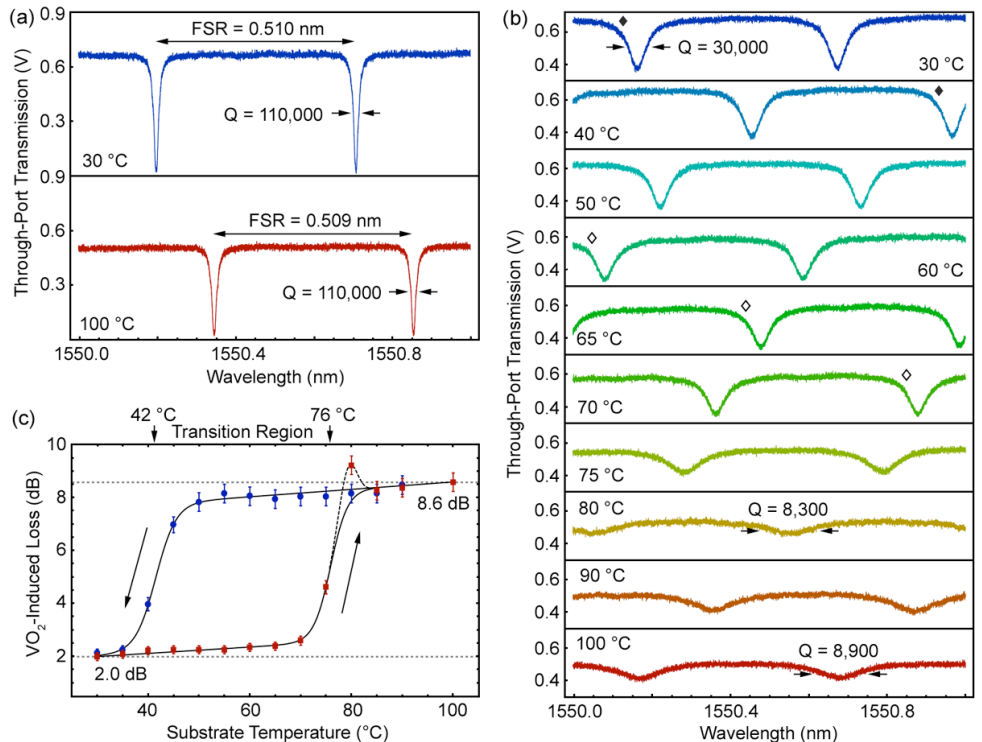


Figure 5. (a) Through-port transmission spectra of a critically coupled Si waveguide ring resonator without a VO₂ tab. The resonator Q is unchanged for substrate temperatures between 30 °C and 100 °C; however, the grating coupling efficiency is impacted by the Si thermo-optic effect, resulting in lower off-resonance transmission. (b) Through-port transmission spectra for increasing substrate temperature for the same resonator geometry, but with a 2- μm long VO₂ tab. Modes of the same azimuthal order are indicated with diamond-shaped markers, revealing a thermally induced redshift of 0.08 nm/°C. (c)

shows strong temperature dependence, consistent with the insulator-to-metal phase transition occurring near 68 °C, as shown in Fig. 5(b). By measuring the decrease in the resonator Q factor, and comparing it with the Q of the reference device, we can quantitatively determine the VO₂-induced loss. The corresponding loss per round-trip is plotted in Fig. 5(c) for temperatures ranging between 30 and 100 °C. The additional loss due to the 2- μ m long VO₂ section in its insulating phase is 2 dB, and the loss is increased to 8.6 dB once the insulator-to-metal phase transition has occurred. Characteristic of polycrystalline VO₂, we also observe broad thermal hysteresis, where the metallic-phase optical properties of the VO₂ are retained upon cooling until around 40 °C. Synthesizing films with smaller crystal grains can reduce the hysteresis; however, broad hysteresis behavior could prove useful for certain devices, such as optical memory elements.

Our device is a compact VO₂-based absorption modulator operating at wavelengths near 1550 nm on a SOI waveguide platform. By directly heating an integrated VO₂-clad waveguide section, we have measured single-pass modulation of 6.6 dB between 30 and 100 °C over a device just 2- μ m long. Electromagnetic simulations show that simply extending the device length to 5 μ m would result in modulation in excess of 16 dB, which is competitive with MZI and electro-absorption modulators, but the insertion loss in the insulating phase would be increased to 5 dB. We envision that future devices will utilize more localized means to induce the phase transition, eliminating the need for a resonator as an accurate temperature-independent probe of modulation. In particular, since the VO₂ phase transition can also be induced athermally, future devices can potentially use local optical or electrical stimulus to not only induce the dramatic shift in absorption observed here, but do so on extremely short time scales.

Color Imaging via Plasmonic Color Filters Integrated onto a CMOS Image Sensor

Plasmonic hole arrays have been the subject of enormous scientific interest over the last 15 years since the first observation of extraordinary light transmission in hole arrays. Since that advance, the physics of hole array spectral filtering has been intensively debated and recently plasmonic hole arrays have been investigated for complementary color imaging applications and densely integrated plasmonic hole array filters have been demonstrated and integrated onto CMOS image sensors. In this project, we demonstrated the imaging characteristics of a 360x320 pixel color camera by integrating a plasmonic color filter array with a commercial black and white 1/2.8 inch CMOS image sensor, and high resolution full color images are taken with the integrated image sensor. The color filters shown in Fig. 6, consisting of 5.6x5.6 μ m² size color pixels in a 150-nm Al film, were chosen to correspond to the RGB primary colors and arranged in a Bayer mosaic layout. The color images are taken with C-mount lenses coupled to the image sensor with focal lengths ranging from 6-50mm, all showing good color fidelity with the 6 color (Red, Green, Blue, Yellow, Magenta, Cyan) averaged CIE Delta-E 2000 = 16.6-19.3 after a white balance and color matrix correction is applied to the raw image over the wide range of f-numbers ranging from 1.8-16. The integrated peak filter transmission efficiencies are measured to be in the 50% range, with a FWHM of 200nm for all three RGB filters – in good agreement with the spectral response of isolated unmounted color filters. We

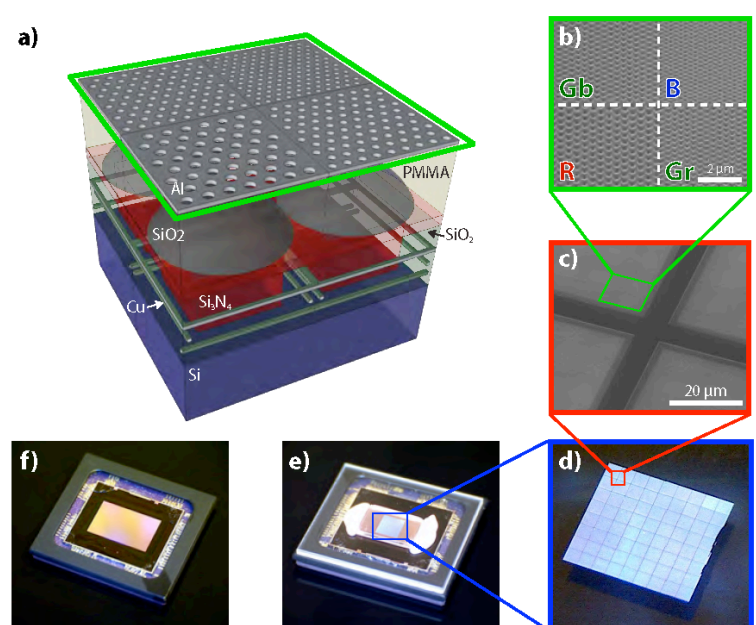


Figure 6. Integrated CMOS image sensor with hole array filter. **a)** Schematic of integrated front-side illumination CMOS image sensor with RGB plasmonic hole array filters in Bayer layout. **b)** Scanning electron micrograph of RGB hole array filters in Bayer layout. **c)** Scanning electron micrograph of 11.2 μ m alignment grid lines separating 40x40 filter blocks. **d)** Image of full 360x320 pixel (2016x1792 μ m²) plasmonic hole array filter array on quartz. Each square on the image corresponds to a 40x40 filter block (224 μ m x 224 μ m²) separated by 11.2 μ m alignment grid lines. **e)** Image of integrated CMOS image sensor with plasmonic hole array filter. The white on the far edges of the filter correspond to electronic grade putty used to hold the filter in place after alignment. **f)** Image of CMOS image sensor before integration.

The integrated peak filter transmission efficiencies are measured to be in the 50% range, with a FWHM of 200nm for all three RGB filters – in good agreement with the spectral response of isolated unmounted color filters. We

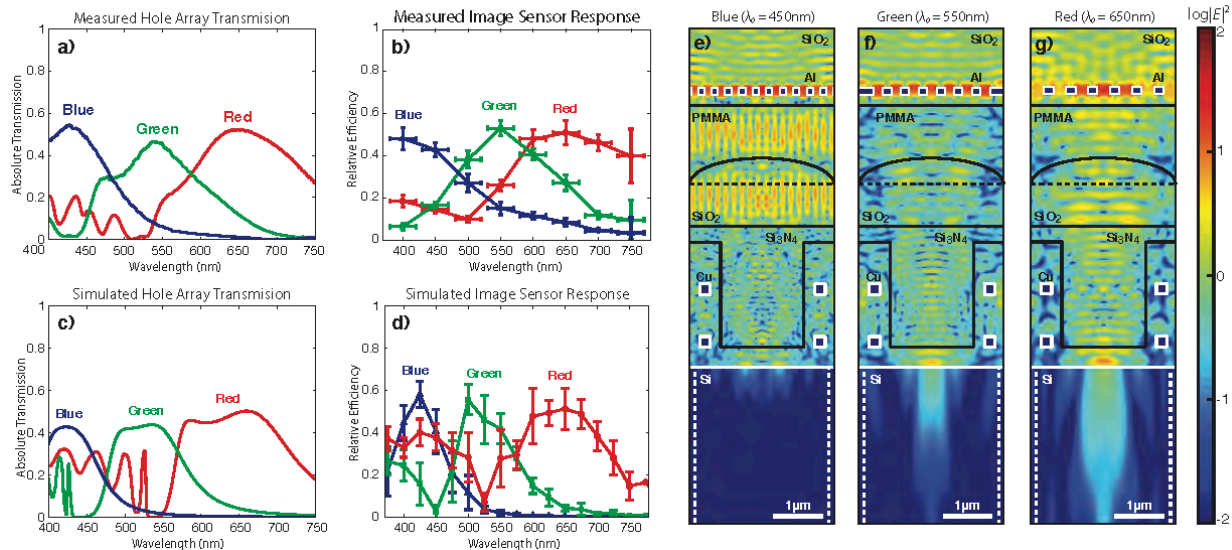


Figure 7. Integrated CMOS image sensor response. **a)** Measured and **c)** simulated spectral response of unmounted RGB plasmonic hole array filters. **b)** Measured and **d)** simulated relative efficiency of integrated CMOS image sensor integrated with RGB plasmonic hole array filters. The horizontal error bars correspond to the spectral width of the band-pass filter used for the measurements and the vertical error bars correspond to the averaged data. Simulation field map cross-sections taken at the center of the pixel and at the center transmission wavelengths for the **e)** blue ($\lambda_0 = 450\text{nm}$), **f)** green ($\lambda_0 = 550\text{nm}$), and **g)** red ($\lambda_0 = 650\text{nm}$) hole array color filters integrated with the CMOS image sensor.

also investigate light coupling from hole array filters to CMOS pixels using full wave electromagnetic simulations.

The optical efficiency of the color filter design was assessed with spectral transmission measurements of isolated $22.4 \times 22.4 \mu\text{m}^2$ size RGB plasmonic hole array filters. The resulting spectra, plotted in Fig. 7a, show all three RGB filter designs having peak efficiencies in the 50-60% range with FWHM in the 150-200nm range, consistent with the transmission data extracted from full field electromagnetic simulations using finite difference time domain calculations for unmounted plasmonic color filters of corresponding dimensions embedded in a quartz matrix illuminated at normal incidence (Fig. 7c).

Using these spectra as a benchmark for the color filter design, the transmission efficiencies of the plasmonic RGB filters as integrated on the CMOS image sensor were estimated by comparing the output signal of the pixels with color filters (corresponding to either R, G, or B) and those without (corresponding to white light). The color bands of interest were selected using narrowband band-pass filters with a FWHM of 40 nm and center wavelengths ranging from 400-750nm in 50nm steps. For each filter, and under constant lighting conditions, an image was taken of a uniform color gray wall using a C-mount lens with a focal length of 12.5mm and an f-number of 5.6. The resulting data is plotted in Fig. 7b.

Direct comparison of the transmission efficiencies between the unmounted (Fig. 7a) and CMOS integrated (Fig. 7b) plasmonic color filters gives a quantitative measurement of how well the plasmonic color filters are integrated onto the CMOS image sensor. In comparing these two data sets, we see that the integrated peak transmission efficiencies are in the 50% range, which is only slightly lower than those of the unmounted color filters – indicating that although the direct contact integration scheme is not optimal, it does not degrade the efficiency significantly. Because the color filter was integrated by simply by pressing the filter and image sensor into intimate contact, we expected that there could be a low refractive gap between the bottom of the plasmonic filter and the top surface of the image sensor that could reduce the light coupling efficiency. However we find from full field electromagnetic simulations of the integrated device that the experimentally measured absolute light coupling efficiencies shown in Fig. 7c are in the same range as those simulated under perfect light coupling conditions in intimate mechanical contact (Fig. 7d), indicating that the integration is nearly ideal.

The resulting simulated steady state intensity field distributions of the three filters at their center wavelengths are shown in Figs. 7e-g, showing that a significant factor in the high light coupling efficiency comes from the nitride waveguide which directs the light into the active region of the Si image sensor pixel.

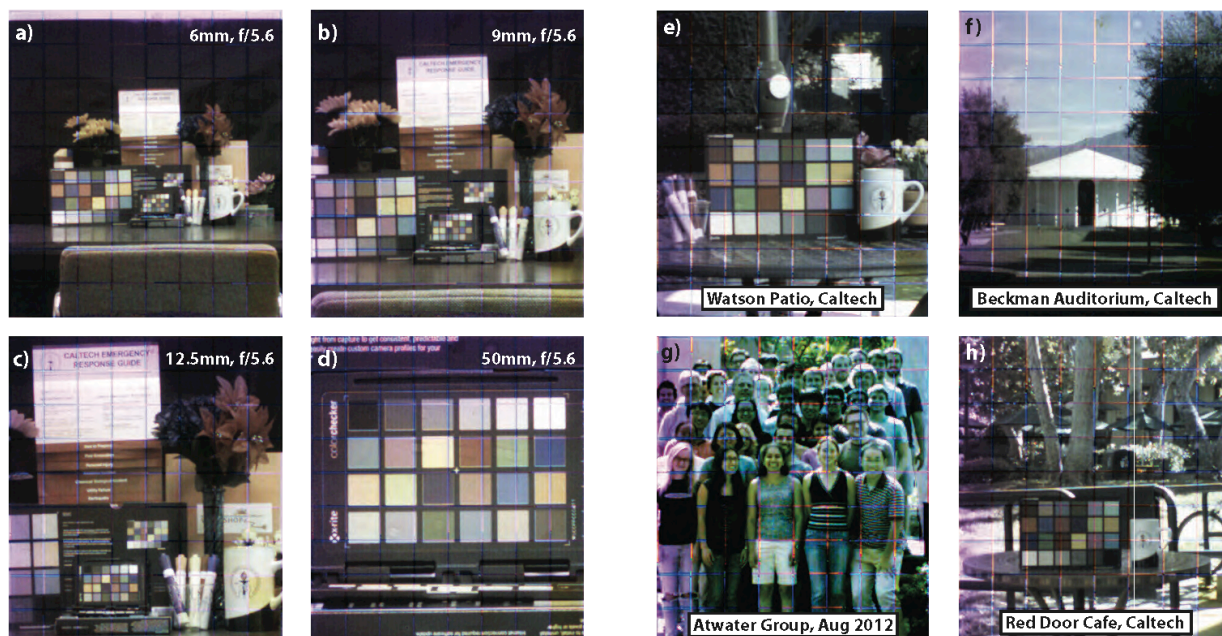


Figure 8. Focal length dependence and outdoor lighting conditions. Images of 24-color Macbeth chart positioned in a scene taken with integrated CMOS image sensor with RGB plasmonic hole array filter with a 5.6 f-number and with lenses with focal length values of **a)** 6mm, **b)** 9mm, **c)** 12.5mm, and **d)** 50mm. Images taken with outdoor lighting conditions of **e)** Watson Patio, Caltech, **f)** Beckman Auditorium, Caltech, **g)** Atwater Group, Aug 2012, Caltech, and **h)** Red Door Café, Caltech.

We note also that as expected the simulations indicate that blue light absorption occurs in the Si pixel near-surface region, while green light absorption occurs at a depth of approximately 1 μm , and red light absorption occurs at a depth of approximately 3 μm below the Si surface. Importantly, the simulations also indicate that the integrated plasmonic filter and image sensor pixel exhibits negligible crosstalk in the form of light scattering into adjacent pixels after light is coupled through the plasmonic filter.

We show in Fig. 8 several images taken with the integrated CMOS image sensor, providing a demonstration of the full-format CMOS imaging camera and color fidelity for focal lengths ranging from 6-50 mm, illustrating the versatility with respect to focal length and outdoor lighting conditions. The spurious lines present in these images are due to alignment marks demarcating fields of the plasmonic filter arrays; these alignments can be omitted in future designs to enable images free from these obscurations.

Enhancing the Radiative Rate in Active Plasmonic Core-Shell Nanowire Resonators

Since Purcell first reported that the enhancement of spontaneous emission is directly proportional to the ratio of the quality factor to the modal volume (Q/V), significant effort has been devoted to the design of optical cavities that effectively enhance radiative emission from semiconductors and molecules. This is traditionally achieved in high- Q dielectric cavities that are restricted to volumes larger $(\lambda/n)^3$, the diffraction limit of light. Plasmonic cavities offer new opportunities: although they generally exhibit low quality factors ($Q < 100$), one can

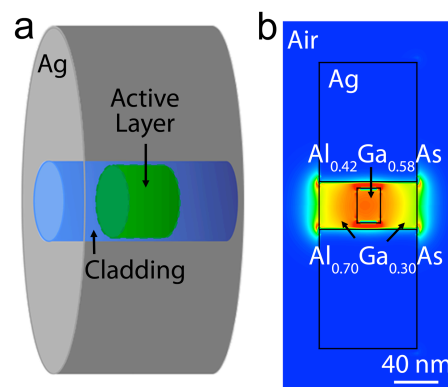


Figure 9. (a) Schematic of a plasmonic core-shell nanowire resonator. The nanowire core consists of a III-V semiconductor active layer clad on all sides with a wider band gap III-V semiconductor and coated with Ag. (b) Cross section showing the lowest order longitudinal mode (near-field electric field intensity) of a structure with $\text{Al}_{0.42}\text{Ga}_{0.58}\text{As}$ active layer and $\text{Al}_{0.70}\text{Ga}_{0.30}\text{As}$ cladding layer.

access ultra-small mode volumes, thereby achieving high Q/V figures of merit.

Our work demonstrated that plasmonic core-shell nanowire resonators, shown schematically in Figure 9a, can access ultra-small mode volumes and dramatically enhance the radiative emission rate of active semiconductor materials in a geometry that can be adapted for an electrically pumped device. Enhancing the emission rate of III-V semiconductors is of particular interest because they have high internal quantum efficiency and an ability to form high-quality heterostructures. In our geometry, the semiconductor heterostructure core has an active light-emitting layer clad on all sides with a wider band gap material and coated with an Ag shell. This geometry allows for significant modification of the local density of optical states (LDOS) simply by changing the material and dimensions of the semiconductor. Thus, we can directly control the total and radiative decay rates inside the active region. Furthermore, we take advantage of the modest quality factors in these plasmonic nanostructures ($Q < 50$) to achieve band-to-band decay rate enhancement. We investigate these structures with GaAs ($\lambda = 870$ nm), $\text{Al}_{0.42}\text{Ga}_{0.58}\text{As}$ ($\lambda = 630$ nm), and $\text{In}_{0.15}\text{Ga}_{0.85}\text{N}$ ($\lambda = 440$ nm) active materials using the boundary element method (BEM). In all cases, the dimensions of the resonator were chosen such that the lowest order longitudinal mode, with high fields and LDOS inside the active layer, would occur at the wavelength λ of band-edge emission from the active semiconductor.

For all three resonators, the mode is highly confined within the core, yielding mode volumes that are approximately equal to the physical volume of the semiconductor. This is illustrated in Figure 9b for the resonator consisting of an $\text{Al}_{0.42}\text{Ga}_{0.58}\text{As}$ active layer and $\text{Al}_{0.70}\text{Ga}_{0.30}\text{As}$ cladding. Here, the peak electric field intensity occurs in the active layer of the device, with fields decaying rapidly at the Ag/ $\text{Al}_{0.70}\text{Ga}_{0.30}\text{As}$ interface, and penetrating only slightly into the surrounding air. This is true for the other two materials systems studied as well ($\text{GaAs}/\text{In}_{0.51}\text{Ga}_{0.49}\text{P}/\text{Ag}$ and $\text{In}_{0.15}\text{Ga}_{0.85}\text{N}/\text{GaN}/\text{Ag}$ as the active/cladding/coating materials). We directly calculate the total decay rate enhancement Γ_{tot} (normalized to decay in vacuum Γ_0) from the LDOS inside the active layer, as well as the radiative decay rate Γ_{rad} (normalized to Γ_0) from the integrated far-field emission due to a dipole located in the center of the resonator core. The smallest resonator system (InGaN/GaN core) has an effective mode volume of $4 \times 10^{-4}(\lambda/n)^3$ and a quality factor of 32, resulting in the largest Q/V figure of merit $7.4 \times 10^4(\lambda/n)^3$ – competitive with conventional high-Q dielectric cavities. The decay rate enhancements and corresponding quantum efficiencies ($\eta = \Gamma_{\text{rad}}/\Gamma_{\text{tot}}$) of the three materials systems (GaAs, AlGaAs, InGaN) are plotted in Figure 10. The largest decay rate enhancements are seen for the $\lambda = 440$ nm mode of the ultra-small InGaN resonator, although significant enhancements are also observed for the GaAs and AlGaAs resonators. Additionally, the quantum efficiencies η at the wavelengths of interest are $>50\%$ for these two resonators. Remarkably, even the smallest resonator (InGaN) maintains a reasonable quantum efficiency $>40\%$, suggesting that a large portion of the enhanced total decay rate correlates to observable photons. The colored shaded regions on the graph correspond to a typical LED bandwidth centered at the emission wavelength of the active material, and because of the moderate quality factors in these plasmonic resonators, the decay rates are enhanced significantly throughout the entire band.

We also calculate the polarization dependence of the far-field radiation at the emission wavelength of each III-V semiconductor plasmonic core-shell nanowire resonator, and compare that to the emission polarization from an uncoated wire, shown in the inset of Figure 10. The far-field radiation is determined for

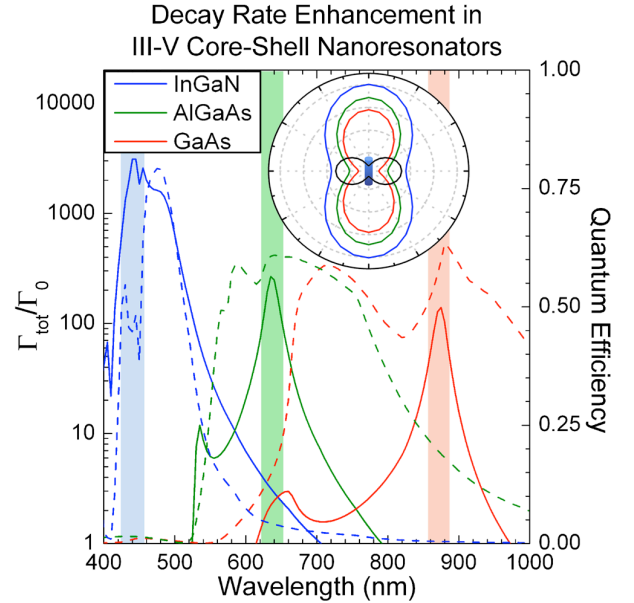


Figure 10. Total decay rate enhancement (solid) and quantum efficiencies (dashed) as a function of wavelength for the three different III-V core-shell nanoresonators. Colored shaded regions indicate typical spectral width of LED emission. (inset) Polar plot of far-field radiation from dipole excitation of the same three core-shell nanoresonators (AlGaAs scaled $\times 35$, GaAs scaled $\times 200$) and in black a bare (uncoated, no Ag) GaAs/InGaP nanowire (scaled $\times 10^5$). The Ag coating modifies both the intensity and direction of the far-field emission.

dipole excitation in the center of the resonator core, and the emission is isotropically averaged for all three dipole orientations. The uncoated wire has a dipolar emission pattern oriented transverse to the longitudinal axis of the nanowire. With the Ag coating, all three of the resonators have a strongly modified emission polarization that is now oriented parallel to the longitudinal axis of the resonator. Thus, the plasmonic coating modifies not only the total and radiative decay rates, but also the direction of far-field radiation. We anticipate that as we continue to shrink resonator dimensions and incorporate new active materials that emit near the surface plasmon resonance, even higher LDOS and radiative decay rate enhancements will be achievable. This work demonstrates that III-V semiconductor plasmonic core-shell nanoresonators are a promising design for fast, bright, nanoscale, and perhaps even directional on-chip light sources.

Plasmonic Enhancement of Spontaneous Emission in GaAs Nanowires

In collaboration with the group of A. Fontcuberta i Morral at EPFL, one area of ongoing work involves designing metal nanostructures to enhance the rate of spontaneous emission from GaAs nanowires inspired by the theoretical results above. Our preliminary experiments include drop casting high quantum efficiency GaAs nanowires grown by molecular beam epitaxy on a variety of substrates (Si, Ag, and Ag coated with a thin Cr layer) and comparing the GaAs photoluminescence (PL) intensity and lifetime decay traces.

Single nanowire spectroscopy is performed with a picosecond super continuum laser source operating at 40 MHz passed through filters for excitation between 550 and 750 nm. The laser is sent through an inverted optical microscope operating in reflection with a 100x objective (0.9 NA) and focused to a 15 μm spot on the nanowire. In the detection path, a CCD and a single photon avalanche diode permit collection of single nanowire PL spectra and PL lifetime decay traces, respectively. Individual GaAs nanowires are approximately 15 μm long, and with a diameter that tapers from 150 to 80 nm. Once drop cast onto the various substrates, PL spectra (Figure 11a) and PL lifetime decays (Figure 11b) are measured for several nanowires. Because of absorption in the Si at both the pump wavelengths and at the PL emission wavelength, the emission intensity for the GaAs nanowire on Si is too low to plot alongside the others in Figure 11a. The PL spectra for nanowires on the other two substrates, however, show a five-fold enhancement in the emission intensity for a nanowire on Ag when compared to a nanowire on Ag+Cr. We expect the thin Cr layer to damp surface plasmon propagation while not significantly diminishing the reflectivity of the Ag, and therefore attribute the PL intensity enhancement to coupling into surface plasmons. Furthermore, the PL decay traces in Figure 11b illustrate shorter PL lifetimes for a GaAs nanowire on Ag ($\tau=43$ ps) compared to nanowires on Si and Ag+Cr ($\tau=125$ ps). We are now exploring this enhancement in greater detail, incorporating a thin MgF_2 spacer layer of varying thickness between the Ag film and the GaAs nanowire. These results encourage further experimental investigation of additional plasmonic nanostructures for enhancing spontaneous emission, a variety of which can be easily fabricated using focused ion beam milling of metal films

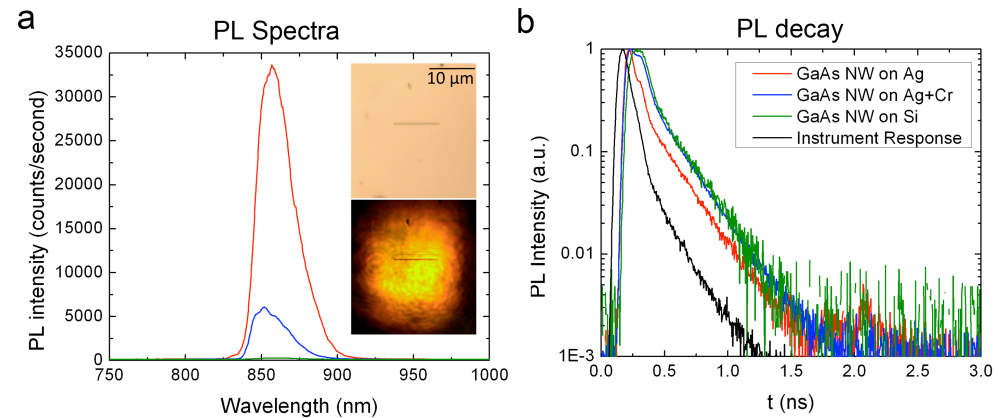


Figure 11. (a) PL intensity and (b) PL lifetime decay for single GaAs nanowires on three substrates: Si (green), Ag (red), and Ag+Cr (blue), with the instrument response for decay measurements plotted in black. The PL spectra show a 5-fold enhancement in PL intensity for a NW on Ag when compared to a NW on Ag+Cr, and the PL decay shows a 3x decay rate enhancement for a NW on Ag compared to NWs on bare Si and Ag+Cr films. Insets in (a): (top) Bright field reflected light image, and (bottom) laser spot focused on a single nanowire.

Single nanowire spectroscopy is performed with a picosecond super continuum laser source operating at 40 MHz passed through filters for excitation between 550 and 750 nm. The laser is sent through an inverted optical microscope operating in reflection with a 100x objective (0.9 NA) and focused to a 15 μm spot on the nanowire. In the detection path, a CCD and a single photon avalanche diode permit collection of single nanowire PL spectra and PL lifetime decay traces, respectively. Individual GaAs nanowires are approximately 15 μm long, and with a diameter that tapers from 150 to 80 nm. Once drop cast onto the various substrates, PL spectra (Figure 11a) and PL lifetime decays (Figure 11b) are measured for several nanowires. Because of absorption in the Si at both the pump wavelengths and at the PL emission wavelength, the emission intensity for the GaAs nanowire on Si is too low to plot alongside the others in Figure 11a. The PL spectra for nanowires on the other two substrates, however, show a five-fold enhancement in the emission intensity for a nanowire on Ag when compared to a nanowire on Ag+Cr. We expect the thin Cr layer to damp surface plasmon propagation while not significantly diminishing the reflectivity of the Ag, and therefore attribute the PL intensity enhancement to coupling into surface plasmons. Furthermore, the PL decay traces in Figure 11b illustrate shorter PL lifetimes for a GaAs nanowire on Ag ($\tau=43$ ps) compared to nanowires on Si and Ag+Cr ($\tau=125$ ps). We are now exploring this enhancement in greater detail, incorporating a thin MgF_2 spacer layer of varying thickness between the Ag film and the GaAs nanowire. These results encourage further experimental investigation of additional plasmonic nanostructures for enhancing spontaneous emission, a variety of which can be easily fabricated using focused ion beam milling of metal films

Personnel Supported:

Faculty: Dr. Harry A. Atwater

Postdocs: Koray Aydin

Graduate Students: Carrie E. Hofmann, Ryan M. Briggs, Stanley Burgos, Imogen Pryce, James Fakonas

Collaborators: Roch Espiau-Lemaestre (LETI Grenoble), Anna Fontcuberta i Morral (EPFL), and Javier Garcia de Abajo (ICFO).

Publications: Peer-reviewed publications submitted and/or accepted during the grant period

1. A. Emboras, R. M. Briggs, A. Najar, S. Nambiar, C. Delacour, Ph. Grosse, E. Augendre, J. M. Fedeli, B. de Salvo, H. A. Atwater, and R. Espiau de Lamaestre, "Efficient coupler between silicon photonic and metal-insulator-silicon-metal plasmonic waveguides", **Applied Physics Letters** **101**, 251117 1-4 (2012).
2. Sozo Yokogawa, Stanley P. Burgos, and Harry A. Atwater, "Plasmonic Color Filters for CMOS Image Sensor Applications", **Nano Letters** **12**, pp 4349–4354 (2012).
3. Stanley P. Burgos, Sozo Yokogawa, and Harry A. Atwater, "Color Imaging via Integrated Plasmonic Color Filters on a CMOS Image Sensor", submitted (2012).
4. Alexandra Boltasseva and Harry A. Atwater, "Low-Loss Plasmonic Metamaterials", **Science** **331**, 290 (2011).
5. Koray Aydin , Vivian E. Ferry , Ryan M. Briggs and Harry A. Atwater, "Broadband polarization-independent resonant light absorption using ultrathin plasmonic super absorbers", **Nature Communications**, **2**:517 | DOI: 10.1038/ncomms1528 , 1-7 (2011).
6. C. E. Hofmann, F. J. Garcia de Abajo, and H. A. Atwater. "Enhancing the radiative rate in III-V semiconductor plasmonic core-shell nanowire resonators," **Nano Letters** **11** 372-376 (2011).
7. Imogen M. Pryce, Koray Aydin, Yousif A. Kelaita, Ryan M. Briggs and Harry A. Atwater, "Characterization of the tunable response of highly strained compliant optical metamaterials", **Phil. Trans. Royal Society A** **369**, 3447-3455 (2011).
8. Imogen M. Pryce, Yousif A. Kelaita, Koray Aydin, and Harry A. Atwater, "Compliant Metamaterials for Resonantly Enhanced Infrared Absorption Spectroscopy and Refractive Index Sensing", **ACS Nano** **5**, 8167-8174 (2011).
9. R. M. Briggs, J. Grandidier, and H. A. Atwater. "Efficient coupling between dielectric-loaded plasmonic and silicon-photonic waveguides," **Nano Letters** **10** 4851-4857 (2010).
10. D. M. O'Carroll, C. E. Hofmann, and H. A. Atwater. "Conjugated polymer/metal nanowire heterostructure plasmonic antennas," **Advanced Materials** **22**, 1223-1227 (2010).
11. R. M. Briggs, I. M. Pryce, and H. A. Atwater. "Compact silicon photonic waveguide modulator based on the vanadium dioxide metal-insulator phase transition," **Optics Express** **18**, 11192-11201 (2010).
12. Feigenbaum, E., K. Diest, et al. (2010). "Unity-Order Index Change in Transparent Conducting Oxides at Visible Frequencies." **Nano Letters** **10** 2111-2116 (2010).
13. Imogen M. Pryce, Koray Aydin, Yousif A. Kelaita, Ryan M. Briggs, and Harry A. Atwater, "Highly Strained Compliant Optical Metamaterials with Large Frequency Tunability", **Nano Letters**, **10**, 4222-4227 (2010).

a. Invited Conference and Seminar Presentations

Listed below is a summary of invited presentations given by the principal investigator on the subject of plasmonic materials and devices under this contract during the period 7/1/09-6/30/12:

H.A Atwater:

2012

1. 6/21/2012- Gordon Research Conference on Noble Metal Nanoparticles, Mount Holyoke College, South Hadley MA.
2. 6/13/2012, Eni Award Lecture, Rome, Italy
3. 6/1/2012- International Workshop on Novel Ideas in Optics: From Advanced Materials to Revolutionary Applications, Purdue University, West Lafayette, IN, USA
4. 5/18/2012 - European Materials Research Society, Strasbourg, France
5. 5/3/2012- Billig-Croft Lecture, Johns Hopkins University, Baltimore, MD
6. 4/24/2012 – SU2P Conference, Edinburgh, Scotland,
7. 4/17/2012 – SPIE Photonics Europe, Brussels, Belgium
8. 4/16/2012 – International Forum on Applied Physics, Trieste, Italy,
9. 4/10/2012 – Spring MRS, Symposium KK, San Francisco, CA “New Directions in Plasmonics.”
10. 4/10/2012 – Spring MRS, Symposium CC San Francisco, CA
11. 3/23/2012 – DOE Sunshot Distinguished Lecture Series. Washington, DC
12. 3/20/2012 – Fourth International Workshop on Thin-Film Silicon Solar Cells , Neuchatel, Switzerland,
13. 3/6/2012 – International Symposium on Innovative Solar Cells, RCAST – Tokyo, Japan,
14. 1/3/2012 – Physics of Quantum Electronics Conference, Snowbird, UT

2011

1. 12/12/2011 – Erlangen, Germany Next Generation Solar Energy Workshop,
2. 11/28/2011– Fall MRS, "Photonic and Plasmonic Materials for Enhanced Photovoltaic Performance", Boston, MA
3. 11/3/2011 – OSA Photovoltaics Workshop, Austin, TX
4. 10/18/2011 – OSA Frontiers in Optics Conference, San Jose, CA
5. 10/10/2011 – (Plenary) Metamaterials 2011 Conference. Barcelona, Spain.
6. 10/5/2011 – (Plenary) Molecular Foundry/NCEM Joint User Meeting, Berkeley, CA
7. 9/22/2011 – (Keynote) Taipei, Taiwan, International Conference in Asia.
8. 8/24/2011 – (Keynote) SPIE Optics and Photonics San Diego, CA
9. 8/8/2011 – ICMR, Emerging Materials for Thin Film Solar Cells, Santa Barbara, CA
10. 7/21/2011 Gordon Research Conference on Crystal Growth and Thin Films, Biddeford, ME
11. 6/20/2011 IEEE Photovoltaic Specialists Conference, Seattle WA
12. 6/3/2011 Nippon Sheet Glass Endowed Lecture, UCLA, Los Angeles CA
13. 5/26/2011 Energy Frontier Center Forum and Summit, Washington DC
14. 5/22/2011 Distinguished Lecture Series in Plasmonics, Seoul National University, Seoul, Korea
15. 5/20/2011 Colloquium, Samsung Advanced Institute of Science and Technology, Suwon, Korea
16. 5/17/2011 5th International Conference on Surface Plasmon Photonics, Pusan, Korea
17. 5/12/2011 (Plenary) Lecture, Argonne Northwestern Solar Energy Research Center, Evanston IL
18. 5/10/2011 (Plenary) Lecture, European Materials Research Society Meeting, Nice, France
19. 5/3/2011 OSA Conference on Lasers and ElectroOptics/Quantum Electronics and Laser Science, Baltimore, MD
20. 5/2/2011 –NRC Condensed Matter and Materials Research Committee Meeting, Washington, DC
21. 4/26/2011 Symposium C, Spring 2011 Materials Research Society Meeting, San Francisco, CA
22. 4/26/2011 Symposium EE, Spring 2011 Materials Research Society Meeting, San Francisco, CA
23. 3/29/2011 American Chemical Society Annual Meeting, Anaheim, CA
24. 3/27/2011 SRC/Masdar Institute Symposium on Solar Electric Energy Systems, Abu Dhabi (by videolink)
25. 3/9/2011 DOE Physical Behavior of Materials Meeting, Airlie VA

26. 1/24/2011 SPIE Photonics West Conference on Synthesis and Photonics of Nanoscale Materials, San Francisco, CA
27. 1/24/2011 SPIE Photonics West Conference on Physics and Simulation of Optoelectronic Devices, San Francisco, CA
28. 1/20/2011 Spitzer Memorial Lecture, University of Southern California, Los Angeles CA
29. 1/15/2011 Kavli Futures Symposium, Pasadena, CA
30. 1/6/2011 Physics of Quantum Electronics, Snowbird, UT

2010

1. 10/30/2010 Symposium M, Fall 2010 Materials Research Society Meeting, Boston MA
2. 10/30/2010 Symposium Y, Fall 2010 Materials Research Society Meeting, Boston MA
3. 10/29/2010 Symposium AA, Fall 2010 Materials Research Society Meeting, Boston MA
4. 10/18/2010 Condensed Matter Physics Seminar, University of California, Berkeley, CA
5. 10/16/2010 Springer Symposium in Applied Physics, Stanford University, Stanford, CA
6. 10/1/2010 Colloquium, Chemical Engineering Department, University of Illinois, Urbana, IL
7. 10/8/2010 Berkeley Nanoscience Seminar, University of California, Berkeley, CA
8. 10/6/2010 Research Seminar, ExxonMobil Research Center, Clinton Township, NJ
9. 10/1/2010 Frontiers in Energy Science and Technology Workshop, Harvard University, Cambridge, MA
10. 9/23/2010 Emtech 2010 Conference at MIT, Cambridge, MA
11. 9/21/2010 4th International Summer School on Physics of Functional Micro- and Nanostructures, Hamburg Germany
12. 9/20/2010 CLEO Europe Conference on Plasmonics and Metamaterials, Turin, Italy
13. 9/8/2010 Colloquium, Mechanical Engineering and Materials Science, Yale University, New Haven CT.
14. 8/24/2010 American Chemical Society National Meeting, Boston, MA
15. 7/6/2010 EFRC Workshop on Light Matter Interactions in Solar Energy Conversion, Pasadena, CA
16. 6/17/2010 Gordon Conference on Plasmonics, Colby College, Waterville ME
17. 6/2/2010 Kavli Royal Society Meeting on Future of Plasmonics, Buckinghamshire, UK
18. 5/31/2010 Summer School on Materials for Renewal Energy Systems, Erice, Italy
19. 4/6/2010 Invited Talk, Symposium D, Spring 2010 Materials Research Society Meeting, San Francisco, CA
20. 4/5/10 Kavli Distinguished Lecture in Nanoscience, Spring 2010 Materials Research Society Meeting, San Francisco, CA
21. 3/31/2010 Colloquium Ehrenfestii Leiden University, Leiden, the Netherlands
22. 3/19/2010 American Physical Society March Meeting, Portland OR
23. 3/17/2010 Materials Science Colloquium, Cornell University, Ithaca NY
24. 2/12/2010 Lunchtime Symposium 2010 TED Conference on Technology, Entertainment and Design, Long Beach, CA
25. 2/3/2010 Center for Energy Efficient Materials Colloquium, UC Santa Barbara, Santa Barbara, CA
26. 1/30/2010 Conference on Mathematics of Technology, Harvey Mudd College, Claremont, CA
27. 1/20/2010 Maddox Lecture, Texas Tech University, Lubbock, TX
28. 1/7/2010 ONR Materials Frontiers Workshop, Naval Research Laboratory, Washington DC
29. 1/5/2010 40th Physics of Quantum Electronics Symposium, Snowbird, UT

2009

1. 12/4/2009 Symposium N, Fall 2009 Materials Research Society Meeting, Boston, MA
2. 12/2/2009 Symposium EE, Fall 2009 Materials Research Society Meeting, Boston, MA
3. 12/1/2009 Symposium I, Fall 2009 Materials Research Society Meeting, Boston, MA
4. 10/13/2009 Materials Science Colloquium, Stanford University, Stanford, CA
5. 10/10/09 (Plenary) Lecture, Gordon and Betty Moore Foundation, Palo Alto, CA
6. 9/29/09 (Plenary) Lecture, DOE Center for Integrated Nanotechnology Meeting, Santa Fe, NM
7. 9/9/09 Invited Talk, Group IV Photonics Conference, San Francisco, CA
8. 8/26/09 Invited Talk, Metamaterials 2009, London, UK
9. 8/5/09 Invited Talk. SPIE Optics and Photonics Conference. San Diego. CA

b. Awards

- Visiting Professorship, Royal Netherlands Academy of Arts and Sciences, 2013
- Eni Award for Renewable and Non-conventional Energy, 2012
- SPIE Green Photonics Award 2012
- Materials Research Society Fellow, 2011
- 2010 Breakthrough Innovation Award, *Popular Mechanics Magazine* (for Si wire array solar cells)
- Fred Kavli Distinguished Lectureship in Nanoscience, Materials Research Society, 2010

c. Consultative and Advisory Functions

- Advisory briefings for Defense Science Research Council and DARPA Defense Sciences Office (DSO).

d. Transitions.

- Developed mask set and CMOS/Plasmonic waveguide process for use in LETI CMOS Si Photonics foundry.
- Develop CMOS color-imaging camera integrated with CMOS image sensor, in collaboration with Sony.